J. Synchrotron Rad. (1998). **5**, 107–111

Time-Resolved Grazing-Incidence Diffraction Studies of Thin Films Using an Imaging-Plate Camera and Focusing Monochromator

Garry J. Foran,[a]*† Ian R. Gentle,[b] Richard F. Garrett,[a] Dudley C. Creagh,[c] Jian Bang Peng[b] and Geoffrey T. Barnes[b]

[a]Australian Nuclear Science and Technology Organisation, PMB 1, Menai, NSW 2234, Australia, [b]Department of Chemistry, University of Queensland, Brisbane, Queensland 4072, Australia, and [c]Faculty of Information Sciences and Engineering, University of Canberra, PO Box 1, Belconnen, ACT 2616, Australia. E-mail: foran@anbf2.kek.jp

(Received 16 September 1997; accepted 27 November 1997)

A multiple imaging-plate (IP) detector system and focusing monochromator have been developed and successfully applied to the time-resolved study of phase transitions in Langmuir–Blodgett (LB) films by grazing-incidence X-ray diffraction (GIXD). The first reported application of imaging plates to a GIXD study was carried out by our group and proved to be very successful in the determination of thin-film structure [Foran, Peng, Steitz, Barnes & Gentle (1996). *Langmuir*, **12**, 774–777]. To extend the capabilities of this system, an IP camera was designed and built which can accommodate up to 13 IPs (40 × 20 cm) inside the vacuum chamber of the main diffractometer at the Australian Beamline at the Photon Factory. The camera allows the enclosed IPs to be successively exposed and stored inside the diffractometer for later scanning. The focusing monochromator employed in this technique combines fixed exit-beam height with sagittal focusing of the second crystal and delivers a gain in flux of >20 times when measured through a 0.1 × 0.1 mm aperture. The utility of the system incorporating the IP camera and the focusing monochromator has been demonstrated through the study of temperature-dependent phase transitions in LB films of metal fatty acids.

Keywords: imaging plates; grazing-incidence X-ray diffraction; Langmuir–Blodgett films; phase transitions.

1. Introduction

The Australian National Beamline Facility (ANBF) has been in operation at the Photon Factory since 1993 (Foran *et al.*, 1994). The primary instrument, a large multi-configuration diffractometer, was originally designed as a high-resolution high-speed powder diffraction camera (Barnea *et al.*, 1992; Garrett, Cookson, Foran *et al.*, 1995). However, its unique combination of imaging-plate (IP) detection and vacuum operation has proven particularly suited to several other techniques, especially grazing-incidence X-ray diffraction (GIXD). The combination of this instrument and a newly developed focusing monochromator has given the ANBF a unique capability in solid surface GIXD.

The application of GIXD to the study of structure in surface layers has been a popular and fruitful area of research in recent years. In particular, GIXD has proved very useful in gaining an understanding of the in-plane periodic structure of Langmuir films at air/water interfaces and Langmuir–Blodgett (LB) films on solid substrates (Als-Nielsen & Möhwald, 1991). The weakness of the diffracted signal from such systems has until now required the use of high-flux X-ray sources such as wiggler beamlines at synchrotron radiation facilities in order to scan a sufficiently large area of reciprocal space, in a reasonable time and at the required resolution. For these measurements, scintillation counters and one-dimensional position-sensitive detectors (linear detectors) fitted with Soller collimating slit assemblies have served to record diffraction patterns by step-scanning over the required area of wavevector transfer (Q) space. Even at a particularly high-flux source like beamline 16A of the Photon Factory in Tsukuba, Japan (a 53-pole wiggler with focusing optics in the beamline) (Kobayakawa *et al.*, 1994), a GIXD experiment for a Langmuir monolayer takes approximately 90 min to scan a typical range of Q-space (Matsushita *et al.*, 1991). In a previous paper we reported the first GIXD results recorded using an imaging-plate detector system and indicated the advantages of this method (Foran *et al.*, 1996). Subsequently we reported results from an improved IP-GIXD system which utilizes an IP camera and a focused incident beam (Peng *et al.*, 1997). In this paper we report a full description of the imaging-plate

† Present address: Australian Beamline, KEK-PF, Oho 1-1, Tsukuba, Ibaraki 305-0801, Japan.

detector system for GIXD experiments that has been developed at the Australian National Beamline Facility (BL-20B) at the Photon Factory including several major improvements over the experimental set-up described in our previous manuscript (Foran *et al.*, 1996).

The major instrumental improvements/additions described herein are the introduction of a focusing monochromator to increase X-ray flux at the sample position and thus reduce exposure times, the implementation of a multiple image-plate camera which operates under vacuum inside the diffractometer, and the addition of a sample stage which makes alignment very reproducible and allows the sample temperature to be controlled over the range from room temperature to approximately 403 K. In addition, improvements have been made to the data transformation equations to correct for slight sample tilt around the axis of the incoming beam, and the ability to record diffraction data in both high- and low-Q_{xy} regions simultaneously has been added.

2. Instrumentation

2.1. *Diffractometer*

The multi-purpose diffractometer in use at the ANBF has been described in detail previously (Barnea *et al.*, 1992; Garrett, Cookson, Foran *et al.*, 1995). This diffractometer is particularly well suited to the type of experiment described herein as it incorporates in one instrument the features of precision, remote-controlled goniometers, a two-dimensional detector system (imaging plates) and the ability to operate in a vacuum environment. A schematic of the ANBF diffractometer in IP-GIXD mode is shown in Fig. 1. The sample stage (see below) is mounted on a goniometer head (Huber 1003) on which all axes were remotely driven and controlled *via* DC encoder micrometers (Oriel) (Garrett, Cookson, Davey *et al.*, 1995). The goniometer head was attached to the stage of the Huber 410 goniometer, the axis of rotation of which defines the centre of the instrument (see Fig. 1). A set of remote-controlled four-jaw slits (Garrett, Cookson, Davey *et al.*, 1995) located on the upstream end of the instrument is used to define the vertical dimensions of the incoming beam.

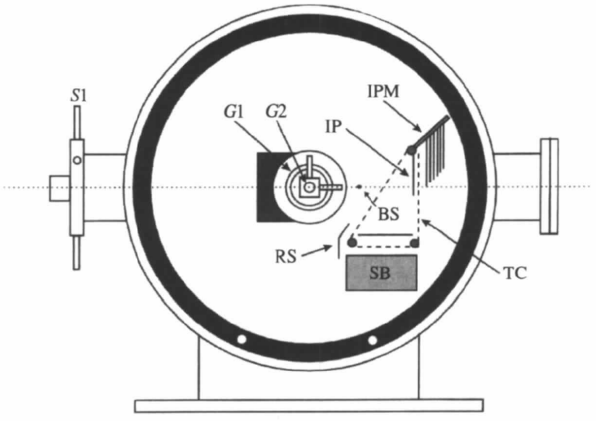

Figure 1
Schematic representation of the diffractometer in IP-GIXD mode. *S*1 = four-jaw slits, *G*1 = Huber 410 goniometer, *G*2 = Huber 1003 motorized goniometer head, IP = imaging-plate/backing-plate assembly in the exposure position, IPM = imaging-plate magazine for unexposed plates, BS = beam stop, SB = storage bin for exposed plates, RS = radiation shielding for storage bin, TC = imaging-plate transport chain.

2.2. *Heating stage*

The heating stage used in the current work is visible in the foreground in Fig. 2. The stage incorporates a 24 V resistance heating element embedded in the main aluminium body of the stage, two *K*-type thermocouples and PTFE retaining lugs for firm reproducible sample mounting. One thermocouple monitors the temperature of the stage body while the other is mounted so as to be in physical contact with an uncoated part of the sample substrate. The stage supports 25 mm × 25 mm wafer samples. The body of the stage is thermally insulated from the stub by which the stage is held in the goniometer head by a sheath of machinable ceramic. The output from one thermocouple was fed to a programmable PID temperature controller which was connected to a DC power supply and interfaced to the beamline control computer to provide remote control of the sample temperature.

2.3. *Imaging-plate camera*

A photograph of the IP camera, which was designed and constructed at the Department of Chemistry workshop at the University of Queensland, is shown in Fig. 2. The primary design parameter for the camera was that it allowed multiple IPs [200 × 400 mm (Fuji)] to be loaded, exposed and stored inside the vacuum chamber of the diffractometer without the need to vent the chamber and re-evacuate between plate exposures. It is crucial also that the exposure position of the IPs be reproducible to avoid errors and allow direct comparison of peak positions from one plate to the next. Before loading into the camera, each IP is fixed to an aluminium backing plate using an alu-

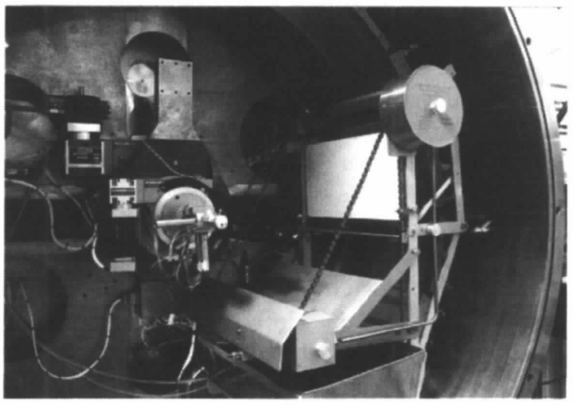

Figure 2
Close-up photograph of the IP camera mounted inside the diffractometer chamber at the Australian Beamline. An IP is visible in the exposure position and the sample stage is in the foreground.

minium frame and locking clips. The role of the backing plate is to provide rigidity for the IPs during exposure and transport and to shield all but the IP in the exposure position from scattered X-rays. Up to 13 of the IP/backing-plate assemblies may be loaded into the camera at any one time. In the exposure position, the IP/backing-plate assembly is held down firmly and reproducibly in two V-shaped slots with the long axis of the IP horizontal. The distance from the centre of the sample to the IP along the beam axis is 400.8 mm. After exposure, the IP/backing-plate assembly is lifted from the exposure position and carried down into a shielded magazine where the IPs are stored until the chamber is vented and the plates removed for scanning. It takes approximately 60 s to remove an exposed plate and lower the next into position.

The size of the IPs and the distance of the detection plane from the sample centre gave at this wavelength (1.739 Å) a measurable Q_{xy} range of 0–2.4 $Å^{-1}$ and a maximum Q_z range of about 0–1.6 $Å^{-1}$. The accessible Q range is of course adjustable by changing the operating wavelength.

2.4. *Monochromator*

The monochromator used in this work combines the features of fixed exit-beam height and sagittally bent second (downstream) crystal. It is positioned 10.9 m from the beam source and the usual focal position is inside the diffractometer at about 14 m, giving approximately the ideal 3:1 focus condition for a sagittally bent crystal (Sparks *et al.*, 1982). The monochromator focuses the X-ray beam to an essentially Gaussian profile spot with ~0.9 mm FWHM at 14 m. The intensity gain was in excess of 20 times when measured as flux into a 0.1 × 0.1 mm aperture with and without focusing.

A detailed description and figures of the monochromator used in this work are presented elsewhere (Foran *et al.*, 1998).

3. Experimental technique and conditions

3.1. *X-ray beam*

The monochromator was set to provide X-rays with a wavelength of 1.739 Å by calibration *versus* the *K*-absorption edge of an iron foil. The beam was then focused on the plane of the imaging-plate detector to a horizontal FWHM of 0.89 mm. The upstream slits (*S*1 in Fig. 1) were set to act as scatter slits in the horizontal direction and to define a beam height of 50 μm in the vertical direction. These settings gave a beam with dimensions 1.6 × 0.05 mm (H × V) at the sample position. The vertical beam size was chosen so as to just cover the full length of the sample surface under grazing-incidence conditions.

3.2. *Alignment*

The samples were mounted on the heating stage such that the surface of the sample was horizontal. Parallelism with the incident beam was checked and adjusted using the motors on the goniometer head and the sample was positioned in the centre of the beam. The angle of incidence of the beam on the sample was set to 0.18° by rotation of the Huber 410 goniometer.

3.3. *Exposure conditions*

Following sample alignment, IP/backing-plate assemblies were loaded into the camera and the diffractometer was sealed and evacuated to a pressure of <1 Torr. Typical exposure times for a single IP were of the order of 2 min although this could be dramatically reduced to about 20 s when the low-Q and/or specular profile were the main area(s) of interest without significant degradation of the signal-to-noise ratio. The ability to scan such a wide area of Q-space in such a short time has until now been impossible for traditional GIXD instrumentation. After the completion of a series of exposures, the diffractometer was vented and the IPs removed from the camera and loaded into magazines for scanning. The imaging plates were scanned on a BAS2000 IP reader (Fuji) at the maximum sensitivity (10000), maximum latitude (4) and with ten-bit AD conversion of the measured intensity. For GIXD measurements employing the IP camera, a pixel size of 100 × 100 μm was used.

When located in the exposure position, the IP is protected from the direct beam (and specularly reflected beam) by a beam stop (BS in Fig. 1). On each scanned image the $Q_z = 0$ line is defined by the projection of the edge of the sample wafer and $Q_{xy} = 0$ is referenced to the position of the specularly reflected profile normal to the surface.

Because there is no enhancement of angular resolution in the IP-GIXD set-up from Soller collimators for example, the resolution in Q of the images varies across the plate and is dependent only on the intrinsic beam divergence and size of the footprint on the sample surface. By focusing the beam horizontally at the image plane and limiting the vertical beam size to <50 μm, suitable resolution of the order of 0.05 $Å^{-1}$ is obtained even at high 2θ angles. Such resolution is quite sufficient for fatty-acid-type LB films where the inherent mosaicity of the samples is regularly 1° or more in 2θ.

3.4. *Data processing*

The raw image files were converted into an array containing linearized intensities and stored as a binary stream using IDL imaging software (RSI, Colorado, USA) running on a Pentium PC. In contrast to our earlier work in which the figure of the IP in the exposure position was a section of a cylinder (Foran *et al.*, 1996), the IPs are held flat in the camera thus simplifying the geometrical transformation that must be calculated to convert the image data to Q-space. Each pixel of the raw data set, with a measured position defined by y_m and z_m, was transformed according to the following equations to obtain the true

scattering angles:

$$2\theta = \tan^{-1}[(y_m \cos\alpha - z_m \sin\alpha)/x],$$

$$\varphi = \tan^{-1}\left\{\frac{y_m \sin\alpha + z_m \cos\alpha}{[x^2 + (y_m \cos\alpha - z_m \sin\alpha)^2]^{1/2}}\right\},$$

where 2θ is the scattering angle in the plane of the sample, φ is the scattered angle in the z (vertical) direction, y_m is the horizontal distance in millimetres of the measured pixel from the centre of the direct beam, z_m is the distance of the measured pixel from the plane of the sample, x is the distance from the centre of the sample to the IP along the path of the direct beam and α is the tilt angle of the sample around the axis of the incident beam. The magnitude of α was typically of the order of $\pm 0.5°$.

These angles were converted to wavevector transfer values using the following relationships:

$$\mathbf{Q} = \mathbf{Q}_{\text{out}} - \mathbf{Q}_{\text{in}},$$

$$Q_z = (2\pi/\lambda)\sin\varphi,$$

$$Q_{xy} = (Q_x^2 + Q_y^2)^{1/2}$$

$$= (2\pi/\lambda)[1 + \cos^2\varphi - 2\cos\varphi\cos(2\theta)]^{1/2},$$

where Q_x, Q_y and Q_z refer to the projections of the wavevector transfer $\mathbf{Q}$ onto the x, y and z axes, respectively. The approximation that $\sin\beta = 0$ and $\cos\beta = 1$ (β = incident angle = 0.18°) has been made in these equations.

3.5. *Samples*

LB films of cadmium arachidate (C_{20} straight-chain fatty acid) were prepared on polished Si(111) substrates (Semiconductor Processing Company, Boston, MA, USA) in vertical deposition mode on a poly(tetrafluoroethylene) trough as reported previously for cadmium stearate films (Peng *et al.*, 1997). The films used in this work consisted of 31 layers of Cd arachidate.

4. Results and discussion

A number of previous studies have reported and investigated the temperature dependence of LB films of cadmium soaps of long-chain fatty acids (Merle *et al.*, 1994, and references therein). Of particular interest has been a phase transition at temperatures around 373 K to a so-called 'columnar' phase (Merle *et al.*, 1994). The first kinetic studies on this transition indicated that the mechanism was not first-order but included at least one intermediate disordered phase (Merle *et al.*, 1991, 1992)

There remains, however, a degree of uncertainty about the structure of the high-temperature phase owing to deficiencies in the reported data. For example, in the SAXS measurements (Merle *et al.*, 1991, 1992) only the (00*l*) diffraction signal (specular direction) was recorded and each of the three *d*-spacings revealed in the electron diffraction measurements (Merle *et al.*, 1994) are from different diffraction photographs of different films. Moreover, as most of these measurements were performed at room temperature after the films had been heated, the structures were not necessarily the same as those existing at the high temperature where the new phase developed and there was certainly no possibility of observing intermediate phases.

Fig. 3 shows a sequence of IP-GIXD images, transformed into Q-space, following the progress of the phase transition which takes place in cadmium arachidate multilayer LB films at around 373 K. The room-tempera-

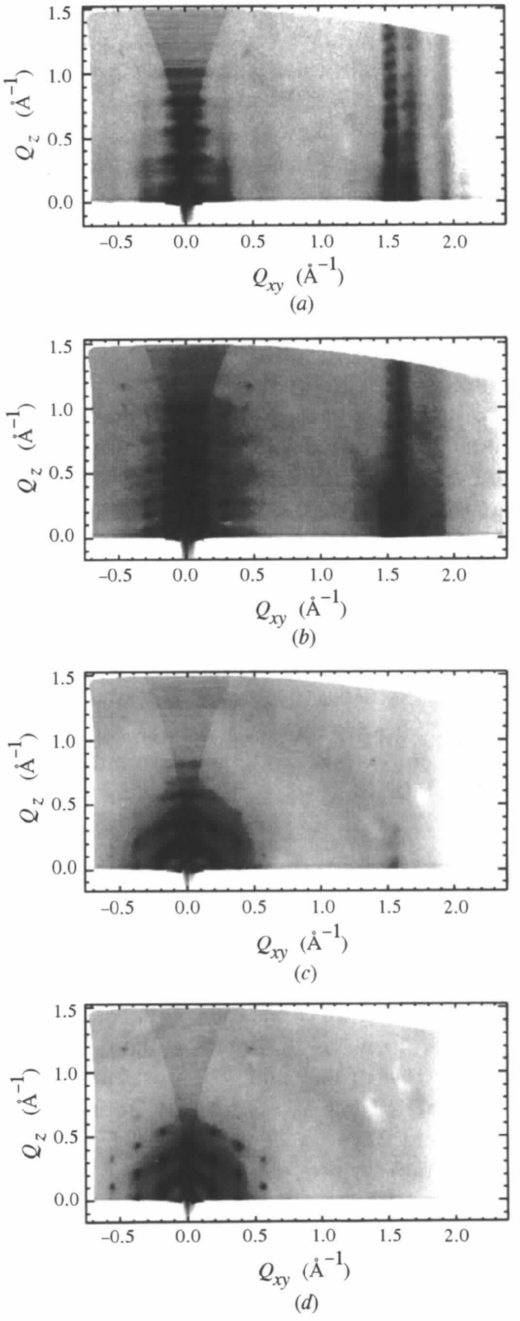

Figure 3
GIXD images of the phase transition in the 31-layer LB film of cadmium arachidate. (*a*) Room temperature, (*b*) 368 K, (*c*) 380 K, (*d*) 383 K. Note the spots due to the intermediate phase in (*b*).

ture image (Fig. 3*a*) shows the characteristic Bragg rods resulting from in-plane diffraction from the centred rectangular arrangement of the fatty-acid molecules, which are aligned normal to the substrate surface, and the rows of spots at fixed Q_z arising from the multilayer nature of the film. The 00*l* diffraction spots along the specular direction are dominant and clearly visible. As the temperature of the sample is raised to 368 K, the relative intensity of the diffraction spots at high Q_{xy} decreases and the spots become diffuse. As can be seen in Fig. 3(*b*) (368 K), this is concurrent with an increasing diffuseness in the 00*l* spots in the Q_z direction and the appearance of spots at low Q_{xy} offset from the 00*l* line. Finally, as the film is annealed at 380 and 383 K, the hexagonal diffraction pattern characteristic of the high-temperature phase appears.

These data, and those which we have published elsewhere (Peng *et al.*, 1997), clearly show the value of the IP-GIXD method as described herein in following phase transitions in thin films and has allowed us to fully characterize the final phase observed here as an array of hexagonally packed rods lying on the surface. The dimensions of the rod cores and the spacings between the rods imply that each rod consists of the polar head groups of the soap chains incorporating the Cd ions, while the aliphatic chains are randomly oriented between the rods.

Moreover, the ability to follow the phase transition *in-situ* has made possible, even in this limited data set, the identification of at least one distinct ordered intermediate, the diffraction signal from which is observable in Fig. 3(*b*). Our most recent data on these systems indicates at least two positively identifiable ordered intermediates in the phase transition of similar Cd soaps (Peng *et al.*, 1998). Data of such detail and quality could not be collected with conventional scanning GIXD instrumentation and further indicates the value of the apparatus described here.

5. Conclusions

The monochromator and detector system described allows the diffraction signal from a monolayer or multilayer sample on a solid substrate to be recorded over a large range of wavevector transfer (Q) space in much shorter times than previously possible with scanning detectors without greatly compromising angular resolution or signal-to-noise. Utilization of the IP camera makes time-resolved GIXD experiments feasible. The usefulness of the technique is demonstrated through the observation and measurement of a temperature-induced phase transition and intermediates in an LB multilayer sample of cadmium arachidate.

The authors acknowledge the assistance and support of Dr David Cookson at the Australian Beamline and the efforts and expertise of the workshop staff of the Chemistry Department at the University of Queensland, in particular Mr Greg Rees and Mr Alan Pringle. This work was supported by the Australian Synchrotron Research Program which has been funded by the Commonwealth of Australia *via* the Major National Research Facilities Program.

References

Als-Nielsen, J. & Möhwald, H. (1991). *Handbook of Synchrotron Radiation*, Vol. 4, edited by S. Ebashi, E. Rubenstein & M. Koch, pp. 1–53. Amsterdam: Elsevier.

Barnea, Z., Creagh, D. C., Davis, T. J., Garrett, R. F., Janky, S., Stevenson, A. W. & Wilkins, S. W. (1992). *Rev. Sci. Instrum.* **63**, 1068–1072.

Foran, G. J., Cookson, D. J. & Garrett, R. F. (1994). *Synchrotron Radiation Facilities in Asia*, edited by T. Ohta, S. Suga & S. Kikuta, pp. 119–124. Tokyo: Ionics Publishing.

Foran, G. J., Garrett, R. F., Gentle, I. R., Creagh, D. C., Peng, J. B. & Barnes, G. T. (1998). *J. Synchrotron Rad.* **5**. In the press.

Foran, G. J., Peng, J. B., Steitz, R., Barnes, G. T. & Gentle, I. R. (1996). *Langmuir*, **12**, 774–777.

Garrett, R. F., Cookson, D. J., Davey, P., Janky, S. & Wilkins, S. W. (1995). *Rev. Sci. Instrum.* **66**, 1684–1686.

Garrett, R. F., Cookson, D. J., Foran, G. J., Sabine, T. J., Kennedy, B. J. & Wilkins, S. W. (1995). *Rev. Sci. Instrum.* **66**, 1351–1353.

Kobayakawa, H., Matsushita, T. & Kihara, M. (1994). *Synchrotron Radiation Facilities in Asia*, edited by T. Ohta, S. Suga & S. Kikuta, pp. 119–124. Tokyo: Ionics Publishing.

Matsushita, T., Iida, A., Takeshita, K., Saito, K., Kuroda, S., Oyanagi, H., Sugi, M. & Furukawa, Y. (1991). *Jpn. J. Appl. Phys.* **30**, L1674–1677.

Merle, H. J., L'vov, Yu. M. & Peterson, I. R. (1991). *Makromol. Chem. Macromol. Symp.* **46**, 271–274.

Merle, H. J., Metzger, H. & Pietsch, U. (1992). *Phys. Scr.* **T45**, 253–255.

Merle, H. J., Steitz, R., Pietsch, U. & Peterson, I. R. (1994). *Thin Solid Films*, **237**, 236–243.

Peng, J. B., Foran, G. J., Barnes, G. T. & Gentle, I. R. (1997). *Langmuir*, **13**, 1602–1606.

Peng, J. B., Foran, G. J., Barnes, G. T. & Gentle, I. R. (1998). To be published.

Sparks, C. J., Ice, G. E., Wong, J. & Batterman, B. W. (1982). *Nucl. Instrum. Methods*, **195**, 73–78.